Technical University of Denmark

DTU

Oscillatory Stability and Eigenvalue Sensitivity Analysis of A DFIG Wind Turbine System

Yang, Lihui; Xu, Zhao; Østergaard, Jacob; Dong, Zhao Yang; Wong, Kit Po; Ma, Xikui

DTU Library
Technical Information Center of Denmark

Oscillatory Stability and Eigenvalue Sensitivity Analysis of A DFIG Wind Turbine System

Lihui Yang, Zhao Xu, *Member, IEEE*, Jacob Østergaard, *Senior Member, IEEE*,
Zhao Yang Dong, *Senior Member, IEEE*, Kit Po Wong, *Fellow, IEEE*, and Xikui Ma

Abstract—This paper focuses on modeling and oscillatory stability analysis of a wind turbine with doubly fed induction generator (DFIG). A detailed mathematical model of DFIG wind turbine with vector-control loops is developed, based on which the loci of the system Jacobian's eigenvalues have been analyzed, showing that, without appropriate controller tuning a Hopf bifurcation can occur in such a system due to various factors, such as wind speed. Subsequently, eigenvalue sensitivity with respect to machine and control parameters is performed to assess their impacts on system stability. Moreover, the Hopf bifurcation boundaries of the key parameters are also given. They can be used to guide the tuning of those DFIG parameters to ensure stable operation in practice. The computer simulations are conducted to validate the developed model and to verify the theoretical analysis.

Index Terms—Doubly fed induction generator (DFIG), eigenvalue sensitivity, Hopf bifurcation, stability.

I. Introduction

DOUBLY fed induction generator (DFIG) is a popular wind turbine system due to its high energy efficiency, reduced mechanical stress on the wind turbine, and relatively low power rating of the connected power electronics converter. The DFIG is also complex involving aerodynamical, electrical, and mechanical systems. With increasing penetration level of DFIG-type wind turbines into the grid, the stability issue of DFIG is of great importance to be properly investigated.

A DFIG system, including induction generator, two-mass drive train, power converters, and feedback controllers, is a

multivariable, nonlinear, and strongly coupled system. Bifurcation phenomena in such a nonlinear system may occur under certain conditions, leading to oscillatory instability. Therefore, practical analysis of DFIG stability will have to involve the bifurcation phenomena. In recent years, some researchers studied stability of industrial motor drives with a wealth of nonlinear dynamics according to the bifurcation and chaos theories [1]–[4]. However, earlier studies mainly deal with dc and simple ac motor drives. The stability analysis of DFIG from a bifurcation perspective is absent.

Eigenvalue analysis of the DFIG wind turbine system has been discussed in [5]–[8], where the participation factor, frequency, and damping ratio analysis are focused. The comprehensive analysis of eigenvalue locus and the eigenvalue sensitivity, which can provide useful guidance in tuning system parameters, have not been carried out earlier.

The Yang *et al.* have investigated the Hopf bifurcation in a vector-controlled DFIG with one-mass drive train [9]. The main purpose of this paper is to study the oscillatory stability of a DFIG system with respect to varying wind speed, and to analyze the eigenvalue sensitivity as well. A more comprehensive system model, incorporating two-mass drive train, pitch control, etc., is developed. Based on this model, the eigenvalue loci are analyzed, revealing that with inappropriate controller parameters, Hopf bifurcation is likely to happen in the system under certain conditions, such as variation of wind speed. Then, eigenvalue sensitivity analysis is carried out to identify possible sources of instability, as well as the key influential parameters with respect to system oscillatory stability. Furthermore, in order to obtain the overview of system oscillatory stability, Hopf bifurcation boundaries with regard to some key parameters are analyzed, in order to facilitate optimal design of the DFIG wind turbine system. This paper focuses on the small-signal-stability analysis of the DFIG wind turbine system itself. The impact of the DFIG on the power system stability will be considered in our future research.

II. Modeling of DFIG Wind Turbine System for Oscillatory Stability Analysis

As shown in Fig. 1 [10], the DFIG system utilizes a wound rotor induction generator in which the stator windings are directly connected to the three-phase grid and the rotor windings are fed through three-phase back-to-back bidirectional pulsewidth modulation (PWM) converters. The back-to-back PWM converters consist of two three-phase six-switch converters, i.e., the rotor- and the grid-side converter, between which a dc-link capacitor is placed. For the wind turbine control level, two stage
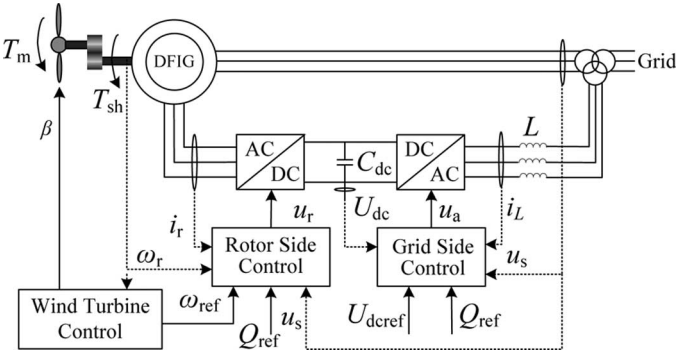
Fig. 1.   Schematic diagram of DFIG wind turbine system.

control strategies, based on the electric power versus wind speed curve, are used for DFIG wind turbines: power optimization strategy below rated wind speed and power limitation strategy above rated wind speed [10]. For the DFIG control level, vector control is used for both the rotor- and the grid-side converters to achieve decoupled control of active and reactive power.

It is recognized that the wind power generations involving DFIG often experience different oscillations resulted from the DFIG and its auxiliary systems [9], [11]. In order to study the oscillatory behavior of the system, small-signal-stability analysis, especially the Hopf bifurcation, is needed. The modeling of DFIG has been studied in [5]–[13]; however, there is currently a lack of a systematic comprehensive modeling approach suitable for small-signal stability. In the following section, we develop a comprehensive model for the DFIG wind turbine system. This model particularly enables small-signal-stability analysis of the overall system.

A. Generator

According to the voltage- and flux-linkage equations of the induction generator [13], [14], the differential equations of the stator and rotor circuits of the induction generator with stator and rotor current as state variables can be given in a d–q reference frame rotating at synchronous speed (we define this reference frame as the generator reference frame in this paper) as follows:

$$
\begin{cases}
\dfrac{di_{ds}}{dt} = D[R_s L_r i_{ds} + (\omega_s - \omega_r)L_m^2 i_{qs} - \omega_s L_s L_r i_{qs} \\
\qquad - R_r L_m i_{dr} - \omega_r L_r L_m i_{qr} - L_r u_{ds} + L_m u_{dr}] \\[4pt]
\dfrac{di_{qs}}{dt} = D[-(\omega_s - \omega_r)L_m^2 i_{ds} + \omega_s L_s L_r i_{ds} + R_s L_r i_{qs} \\
\qquad + \omega_r L_r L_m i_{dr} - R_r L_m i_{qr} - L_r u_{qs} + L_m u_{qr}] \\[4pt]
\dfrac{di_{dr}}{dt} = D[-R_s L_m i_{ds} + \omega_r L_s L_m i_{qs} + R_r L_s i_{dr} \\
\qquad + \omega_s L_m^2 i_{qr} - (\omega_s - \omega_r)L_s L_r i_{qr} + L_m u_{ds} - L_s u_{dr}] \\[4pt]
\dfrac{di_{qr}}{dt} = D[-\omega_r L_s L_m i_{ds} - R_s L_m i_{qs} - \omega_s L_m^2 i_{dr} \\
\qquad + (\omega_s - \omega_r)L_s L_r i_{dr} + R_r L_s i_{qr} + L_m u_{qs} - L_s u_{qr}]
\end{cases}
\tag{1}
$$

where $\mathbf{i}_s = i_{ds} + ji_{qs}$ and $\mathbf{i}_r = i_{dr} + ji_{qr}$ are the stator and rotor current vectors, respectively; $\mathbf{u}_s = u_{ds} + ju_{qs}$ and $\mathbf{u}_r = u_{dr} + ju_{qr}$ are the stator and rotor voltage vectors, respectively; $D = \omega_b/(L_m^2 - L_s L_r)$. This paper adopts the motor convention meaning that stator and rotor currents are positive when flowing into the generator. The quantities in the system model are in per unit except the time t.

B. Drive Train

When studying the stability of DFIG wind turbine, the two-mass model of the drive train is important, as the wind turbine shaft is relatively softer than the typical steam turbine shaft in conventional power plants [15]. The equations, which represent the two-mass model of the drive train, are expressed as follows:

$$
\frac{d\omega_r}{dt} = \frac{1}{2H_g}(T_{\text{sh}} - T_e - B\omega_r)
\tag{2}
$$

$$
\frac{d\theta_t}{dt} = \omega_b(\omega_t - \omega_r)
\tag{3}
$$

$$
\frac{d\omega_t}{dt} = \frac{1}{2H_t}(T_m - T_{\text{sh}})
\tag{4}
$$

where ω_b, ω_r, and ω_t are the base, generator, and wind turbine speeds, respectively. H_g and H_t [SI unit(s)] are the generator and turbine inertias, respectively. θ_t is the shaft twist angle. The electromagnetic torque T_e, the shaft torque T_{sh}, and the mechanical torque T_m, which are the power input of the wind turbine, are as follows:

$$
T_e = L_m(i_{ds}i_{qr} - i_{qs}i_{dr})
\tag{5}
$$

$$
T_{\text{sh}} = K_{\text{sh}}\theta_t + D_{\text{sh}}\omega_b(\omega_t - \omega_r)
\tag{6}
$$

$$
T_m = \frac{0.5\rho\pi R^2 C_p(\lambda,\beta)V_w^3}{\omega_t}
\tag{7}
$$

where C_p is the power coefficient as follows:

$$
C_p = 0.22\left(\frac{116}{\lambda_i} - 0.4\beta - 5\right)e^{-12.5/\lambda_i}
\tag{8}
$$

$$
\lambda_i = \frac{1}{1/(\lambda + 0.08\beta) - 0.035/(\beta^3 + 1)}
\tag{9}
$$

where $\lambda = \omega_t R/V_w$ is the blade tip speed ratio. $C_p(\lambda, \beta)$ has a maximum $C_p^{\max}$ for a particular tip speed ratio λ_{opt} and pitch angle β_{opt}. The aim for variable wind turbine at wind speeds lower than rated value is to adjust the rotor speed at varying wind speeds; therefore, λ and C_p are always maintained at the optimal and maximum value, respectively. The speed control of the DFIG is achieved by driving the generator speed along the optimum power-speed characteristic curve [10], which corresponds to the maximum energy capture from the wind. In this curve, when generator speed is less than the low limit or higher than the rated value, the reference speed is set to the minimal value or rated value, respectively. When generator speed is between the lower limit and the rated value, the rotor speed reference can be obtained by substituting $\lambda = \omega_t R/V_w$ into (7) as follows:

$$
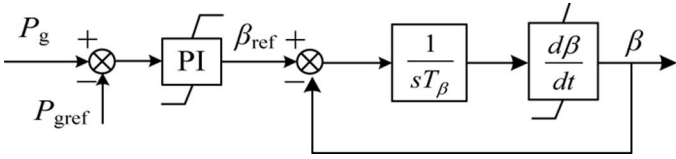\omega_{\text{ref}} = \sqrt{\frac{T_m}{K_{\text{opt}}}}
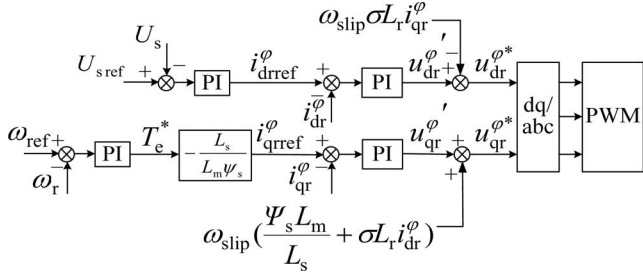\tag{10}
$$

Fig. 2. Schematic diagram of the pitch control.

Fig. 3. Control scheme of the rotor-side converter.

where $K_{\rm opt} = \frac{\rho \pi R^5 C_p^{\max}}{2 \lambda_{\rm opt}^3}$ is the optimal constant of wind turbine. Equation (10) is an easy and direct way to get $\omega_{\rm ref}$ from the academic perspective while it implies the mechanical torque observer is needed. Although mechanical torque observation is not popularly used in industrial application, due to some engineering problems, it is available in practice and can obtain improved optimum operating point tracking [16], [17].

C. Pitch Control

The pitch angle of the blade is controlled to optimize the power extraction of wind turbine as well as to prevent overrated power production in strong wind. The pitch servo is modeled as follows:

$$\frac{d\beta}{dt} = \frac{1}{T_\beta}(\beta_{\rm ref} - \beta). \tag{11}$$

For the sake of simplicity, the reference of the pitch angle $\beta_{\rm ref}$ is kept zero when wind speed is below rated value. When wind speed is higher than rated value, the power limitation is active by adjusting the pitch angle using the pitch-control scheme shown in Fig. 2 [10], and

$$\begin{cases} \beta_{\rm ref} = K_{P\beta}(P_g - P_{\rm ref}) + x_\beta \\ \dot{x}_\beta = \frac{K_{P\beta}}{T_{I\beta}}(P_g - P_{\rm ref}). \end{cases} \tag{12}$$

D. Rotor-Side Converter

The generic control scheme of the rotor-side converter is illustrated in Fig. 3. In order to decouple the electromagnetic torque and the rotor excitation current, the induction generator is controlled in the stator-flux-oriented reference frame, which is a synchronously rotating reference frame, with its d-axis oriented along the stator-flux vector position [17]. The typical proportional–integral (PI) controllers are used for regulation in both the rotor speed and the terminal voltage (outer) control loop
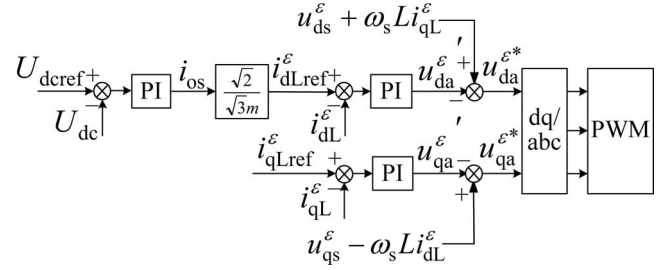
Fig. 4. Control scheme of the grid-side converter.

and the rotor current (inner) control loop. In Fig. 3, superscript φ denotes the variable is in the stator-flux-oriented reference frame.

Based on the stator-flux orientation, the stator flux can be described as $\psi_{ds}^\varphi = \Psi_s$ and $\psi_{qs}^\varphi = 0$ [17]. Accordingly, the rotor-voltage equations can be expressed as follows:

$$\begin{cases} u_{dr}^\varphi = R_r i_{dr}^\varphi - \sigma L_r i_{qr}^\varphi (\omega_s - \omega_r) + \frac{\sigma L_r}{\omega_b} \frac{di_{dr}^\varphi}{dt} \\ u_{qr}^\varphi = R_r i_{qr}^\varphi + \left(\sigma L_r i_{dr}^\varphi + \frac{L_m}{L_s} \Psi_s \right) (\omega_s - \omega_r) + \frac{\sigma L_r}{\omega_b} \frac{di_{qr}^\varphi}{dt} \end{cases} \tag{13}$$

where $\sigma = 1 - (L_m^2 / L_s L_r)$ is the leakage factor.

Usually, the bandwidth of the inner current-control loop is much wider than the outer speed-control loop [17]. Hence, the fast dynamics of the current-control loop does not affect the low-frequency oscillations. On account of this, we assume that the rotor current can well track the reference current, and thus, omit the dynamics of the rotor current-control loop. Under this assumption and according to the control scheme of the rotor-side converter shown in Fig. 3, the equations with respect to the control of the rotor-side converter become

$$\begin{cases} \dot{x}_\omega = \frac{K_{P\omega}}{T_{I\omega}}(\omega_{\rm ref} - \omega_r) \\ \dot{x}_{us} = \frac{K_{Pus}}{T_{Ius}}(U_{\rm sref} - U_s) \\ i_{dr}^\varphi = i_{drref}^\varphi = K_{Pus}(U_{\rm sref} - U_s) + x_{us} \\ i_{qr}^\varphi = i_{qrref}^\varphi = -\frac{L_s}{L_m \Psi_s}[K_{P\omega}(\omega_{\rm ref} - \omega_r) + x_\omega] \end{cases} \tag{14}$$

where $K_{P\omega}$ and $T_{I\omega}$ are the proportional gain and the integral time constant of the rotor-speed controller, respectively.

The rotor voltage in the generator reference frame can be derived by the following: [18]

$$\begin{bmatrix} u_{dr} \\ u_{qr} \end{bmatrix} = \begin{bmatrix} \cos\varphi & -\sin\varphi \\ \sin\varphi & \cos\varphi \end{bmatrix} \begin{bmatrix} u_{dr}^\varphi \\ u_{qr}^\varphi \end{bmatrix} \tag{15}$$

where $\varphi = \arctan(\psi_{qs}/\psi_{ds})$ is the angle between the stator-flux vector and the d-axis of the generator reference frame.

E. Grid-Side Converter

Fig. 4 shows the control scheme of the grid-side converter. In order to obtain the independent control of active and reactive power flowing between the grid and the grid-side converter, the

converter control operates in the grid-voltage-oriented reference frame, which is a synchronously rotating reference frame, with its d-axis oriented along the grid-voltage vector position [17]. Similarly, the typical PI controllers are used for regulation in both dc-link voltage (outer) control loop and grid-side inductor current (inner) control loop. In Fig. 4, superscript ε denotes the variable is in the grid-voltage-oriented reference frame.

Under the grid-voltage-oriented reference frame, the equations of the grid-side converter are given by [17] the following:

$$
\begin{cases}
u_{ds}^{\varepsilon} = U_s = R_L i_{dL}^{\varepsilon} + \dfrac{L}{\omega_b}\dfrac{di_{dL}^{\varepsilon}}{dt} - \omega_s L i_{qL}^{\varepsilon} + u_{da}^{\varepsilon} \\[2mm]
u_{qs}^{\varepsilon} = 0 = R_L i_{qL}^{\varepsilon} + \dfrac{L}{\omega_b}\dfrac{di_{qL}^{\varepsilon}}{dt} + \omega_s L i_{dL}^{\varepsilon} + u_{qa}^{\varepsilon}
\end{cases}
\tag{16}
$$

where $\mathbf{i}_L = i_{dL} + ji_{qL}$ is the grid-side-inductor-current vector, and $\mathbf{u}_a = u_{da} + ju_{qa}$ is the grid-side converter voltage vector.

Similar to the derivation of the rotor-side controller, based on the same simplification, which omits the fast dynamics in the inner current-control loop, and according to the control scheme of the grid-side converter shown in Fig. 4, the equations with respect to the control of the grid-side converter are described as follows:

$$
\begin{cases}
\dot{x}_v = \dfrac{K_{Pv}}{T_{Iv}}(U_{dcref} - U_{dc}) \\[2mm]
i_{qL}^{\varepsilon} = I_{qLref} \\[2mm]
i_{dL}^{\varepsilon} = i_{dLref}^{\varepsilon} = \dfrac{\sqrt{2}}{\sqrt{3}m}[K_{Pv}(U_{dcref} - U_{dc}) + x_u]
\end{cases}
\tag{17}
$$

where K_{Pv} and T_{Iv} are the proportional gain and the integral time constant of the dc-link voltage controller, respectively.

The relationship between the generator reference frame and the grid-voltage-oriented reference frame can be given by [18] the following:

$$
\begin{bmatrix} V_{da} \\ V_{qa} \end{bmatrix} = \begin{bmatrix} \cos\varepsilon & -\sin\varepsilon \\ \sin\varepsilon & \cos\varepsilon \end{bmatrix} \begin{bmatrix} V_{da}^{\varepsilon} \\ V_{qa}^{\varepsilon} \end{bmatrix}
\tag{18}
$$

where $\varepsilon = \arctan(u_{qs}/u_{ds})$ is the angle between the grid-voltage vector and the d-axis of the generator reference frame; V can be the variable of voltage u or current i.

F. DC-link Capacitor

The equation, which describes the energy balance of the dc-link capacitor can be expressed as follows:

$$
\begin{aligned}
\frac{C_{dc}U_{dc}}{\omega_b}\frac{dU_{dc}}{dt} &= p_a - p_r \\
&= \frac{3}{2}(u_{da}i_{dL} + u_{qa}i_{qL} - u_{dr}i_{dr} - u_{qr}i_{qr})
\end{aligned}
\tag{19}
$$

where U_{dc} is the dc-link voltage, and p_a and p_r are the powers supplied to the grid-side converter and the rotor circuit, respectively.

From (1)–(19), we can obtain a set of state equations to present the DFIG wind turbine system. They can be written in a compact form as follows:

$$
\dot{\mathbf{x}} = f(\mathbf{x}, \mathbf{u})
\tag{20}
$$

where $\mathbf{x}$ and $\mathbf{u}$ are the vectors with respect to the state and the input variables, which are defined as $\mathbf{x} = [i_{ds}\ i_{qs}\ i_{dr}\ i_{qr}\ \omega_r\ U_{dc}\ x_\omega\ x_u\ \theta_t\ \omega_t\ \beta\ x_{us}\ x_\beta]^T$, $\mathbf{u} = [u_{ds}\ u_{qs}\ I_{qLref}\ U_{dcref}\ V_w\ \beta_{ref}]^T$.

III. SMALL-SIGNAL-STABILITY ANALYSIS

A DFIG wind turbine system, modeled by (1)–(19) or simply (20), can be linearized to form the linear model around an equilibrium point for small-signal-stability analysis.

A. System Jacobian

The Jacobian matrix is of great importance to stability analysis of dynamical systems. In order to analyze the Jacobian matrix, the equilibrium point X_0 of the system needs to be calculated by solving equation $f(x, u) = 0$. With X_0, the Jacobian matrix of the system evaluated at the equilibrium point is given in (21), shown at the bottom of this page, where $\{J_{i,j}\}$ ($i =$

$$
J(X_0) = \mathbf{A} = \left.\frac{\partial f}{\partial x}\right|_{x=X_0} =
\begin{bmatrix}
J_{11} & J_{12} & J_{13} & J_{14} & J_{15} & 0 & J_{17} & 0 & J_{19} & J_{110} & J_{111} & J_{112} & 0 \\
J_{21} & J_{22} & J_{23} & J_{24} & J_{25} & 0 & J_{27} & 0 & J_{29} & J_{210} & J_{211} & J_{212} & 0 \\
J_{31} & J_{32} & J_{33} & J_{34} & J_{35} & 0 & J_{37} & 0 & J_{39} & J_{310} & J_{311} & J_{312} & 0 \\
J_{41} & J_{42} & J_{43} & J_{44} & J_{45} & 0 & J_{47} & 0 & J_{49} & J_{410} & J_{411} & J_{412} & 0 \\
J_{51} & J_{52} & J_{53} & J_{54} & J_{55} & 0 & 0 & 0 & J_{59} & J_{510} & 0 & 0 & 0 \\
J_{61} & J_{62} & J_{63} & J_{64} & J_{65} & J_{66} & J_{67} & J_{68} & J_{69} & J_{610} & J_{611} & J_{612} & 0 \\
0 & 0 & 0 & 0 & J_{75} & 0 & 0 & 0 & 0 & J_{710} & J_{711} & 0 & 0 \\
0 & 0 & 0 & 0 & 0 & J_{86} & 0 & 0 & 0 & 0 & 0 & 0 & 0 \\
0 & 0 & 0 & 0 & 0 & 0 & 0 & 0 & 0 & J_{910} & 0 & 0 & 0 \\
0 & 0 & 0 & 0 & J_{105} & 0 & 0 & 0 & J_{109} & J_{1010} & J_{1011} & 0 & 0 \\
J_{1101} & J_{1102} & 0 & 0 & 0 & J_{116} & 0 & J_{118} & 0 & 0 & J_{1111} & 0 & J_{1113} \\
0 & 0 & 0 & 0 & 0 & 0 & 0 & 0 & 0 & 0 & 0 & 0 & 0 \\
J_{131} & J_{132} & 0 & 0 & 0 & J_{136} & 0 & J_{138} & 0 & 0 & 0 & 0 & 0
\end{bmatrix}
\tag{21}
$$

1, 2, ..., 4 and $j = 1, 2, ..., 13$) represents the linearized dynamics of the generator from (1); $\{J_{i,j}\}$ ($i = 5, 9, 10$ and $j = 1, 2, ..., 13$) represents the linearized dynamics of the drive train from (2)–(4); $\{J_{i,j}\}$ ($i = 6, 7, 8, 12$ and $j = 1, 2, ..., 13$) represents the linearized dynamics of the dc-link capacitor and controllers of the back-to-back converters from (14), (17), and (19); $\{J_{i,j}\}$ ($i = 11, 13$ and $j = 1, 2, ..., 13$) represents the linearized dynamics of the pitch control from (11) and (12). The elements of the Jacobian matrix are given in the Appendix.

In this paper, we focus on the oscillatory stability analysis of the DFIG itself, the studied DFIG is directly connected to the infinite bus and the dynamic behavior of the grid is not concerned. Therefore, in (14), we have $U_s = U_{s\mathrm{ref}}$, and the differential equation associated with the voltage-control loop can be omitted. Under this assumption, 12th row and 12th column of the Jacobian matrix can be removed. When wind speed is lower than the rated value, the power limitation is not active; therefore, 13th row and 13th column of matrix $J(X_0)$, which are associated with pitch-control loop, can be deleted.

B. Hopf Bifurcation

This paper concentrates on the analysis of local bifurcations, particularly Hopf bifurcation that can occur in a DFIG system.

Hopf bifurcation corresponds to emergence of a periodic solution from an equilibrium point of (20); in this way, the HFB is responsible for system oscillatory behavior. According to the Hopf bifurcation theorem [19], a HFB can be supercritical or subcritical. A supercritical HFB has the initially stable periodic solution branch and will result in a smooth transition to oscillations. On the other hand, a subcritical HFB is associated with an unstable periodic solution branch and will lead to a hard transition to large amplitude oscillations.

The DFIG wind turbine system works in power-optimization operation mode at most of the time. Under this operation mode, the rotor speed of DFIG usually changes along with the variation of wind speed [10]. We will consequently focus on the effect of the variation of wind speed as well as rotor speed on the dynamical behavior of DFIG under the power optimization operation mode in the following section.

C. Eigenvalue Sensitivity

Eigenvalue sensitivity, defined as the rate and direction of eigenvalue movement in the s-plane due to the variation in system parameters is an efficient tool for designing the control system and parameterizing the system, especially for the higher order systems. Two types of eigenvalue sensitivities are studied: eigenvalue sensitivity with respect to the entry of system state matrix and system parameter.

The participation factor is a special group of eigenvalue sensitivity with respect to the system states [20] as follows:

$$P_{ki} = \frac{\partial \lambda_i}{\partial a_{kk}} = u_{ki} v_{ki} (i, k = 1, 2, ..., n) \qquad (22)$$

where a_{kk} is the kth row and kth column of $\mathbf{A}$, $u_i, v_i \in R^n$ denote the normalized right and left eigenvectors corresponding to λ_i, respectively.

TABLE I
SYSTEM PARAMETERS USED IN SIMULATIONS

Parameters	Descriptions	Values
R_s, L_{ls}	Stator resistance and leakage inductance	0.0076 p.u., 0.171 p.u.
R_r, L_{lr}	Rotor resistance and leakage inductance	0.005 p.u., 0.156 p.u.
L_m	Stator and rotor mutual inductance	3.5 p.u.
n_p	Number of pole pairs	3
U_s	Peak amplitude of stator voltage	1 p.u.
ω_s	Stator angular frequency	1 p.u.
H_g	Inertia constant of generator	0.5 s
B	Friction coefficient of generator	0.01 p.u.
H_t	Inertia constant of wind turbine	4 s
K_{opt}	Optimal constant of wind turbine	0.579
T_β	Time constant of the pitch servo	0.25 s
f_{switch}	Switching frequency of the PWM converters	2 kHz
C_{dc}	DC-link capacitance	0.06 F
R_L, L	Resistance and inductance of grid side inductor	0.003 p.u., 0.3 p.u.
U_{dcref}	DC-link voltage reference	1200 V
P_{rated}	Rated power	1.5 MW
ω_{rated}	Rated rotor speed of generator	1.1 p.u.
V_{wrated}	Rated wind speed	12 m/s
ω_b	Base angular frequency	314 rad/s
S_b	Base power	1.5 MW
U_b	Base voltage	575 V

TABLE II
EIGENVALUES OF DFIG WIND TURBINE SYSTEM ($V_w = 12$ M/S, $K_{P_\omega} = 1$)

	$\lambda_{1,2}$	$\lambda_{3,4}$	$\lambda_{5,6}$	$\lambda_{7,8}$
$\lambda = \sigma + j\omega$	-6.84±j314.0	-2.76±j58.8	-5.47±j29.4i	-0.164±j1.43
	λ_9	λ_{10}	λ_{11}	
$\lambda = \sigma + j\omega$	-34.1	-14.1	-4.00	

The first-order sensitivity of an eigenvalue λ_i with regard to a system-operating parameter α can be given by the following:

$$\frac{\partial \lambda_i}{\partial \alpha} = \frac{u_i^T (\partial \mathbf{A}/\partial \alpha) v_i}{u_i^T v_i}. \qquad (23)$$

The magnitude and the sign of the real part of the eigenvalue sensitivity $S_\alpha^{\lambda, \sigma}$ are defined as the size and direction of movement of eigenvalue λ_i in the horizontal direction in the s-plane due to the small perturbation of a general parameter α, respectively, whereas the imaginary part of the eigenvalue sensitivity $S_\alpha^{\lambda, \omega}$ are associated with the movement of eigenvalue λ_i in the vertical direction.

IV. THEORETICAL SYSTEM EIGENVALUE ANALYSIS

Using the Jacobian matrix derived in Section III, eigenvalue analysis of the DFIG wind turbine system is given in this section.

A. Eigenvalue Loci

The system parameters, set as the standard value from MATLAB vR2007b Demo, are detailed in Table I. Using the Jacobian matrix (21), eigenvalues of the DFIG system can be calculated. All the eigenvalues at rated wind speed ($V_w = 12$ m/s, $\omega_r = 1.1$ p.u., $K_{P_\omega} = 1$) are listed in Table II. The eigenvalue loci of corresponding oscillatory modes are plotted in Figs. 5 and 6.

Fig. 5(a)–(d) shows the eigenvalue loci of $\lambda_{1,2}$, $\lambda_{3,4}$, $\lambda_{5,6}$, and $\lambda_{7,8}$ as wind speed increases when $K_{P_\omega} = 60$. The arrows in
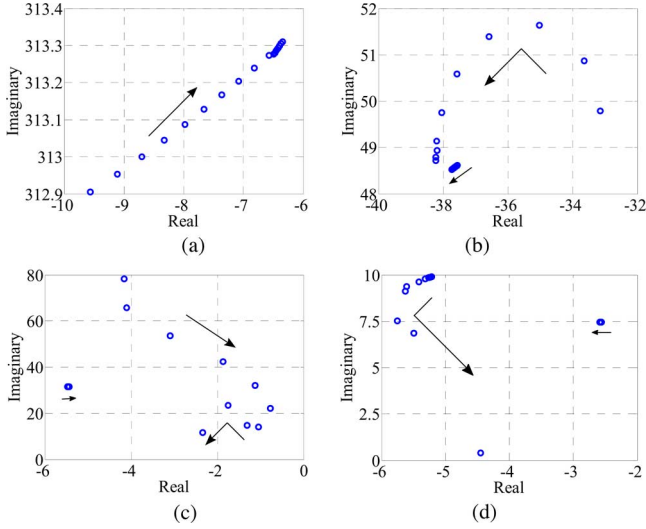
Fig. 5. Eigenvalue loci as wind speed increases from 8 to 15 m/s ($K_{P\omega} = 60$) for (a) $\lambda_{1,2}$, (b) $\lambda_{3,4}$, (c) $\lambda_{5,6}$, and (d) $\lambda_{7,8}$.
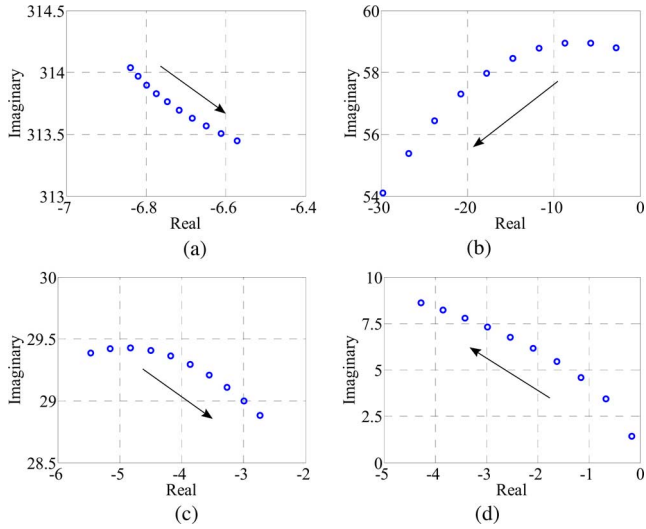

Fig. 6. Eigenvalue loci as the proportional gain of rotor speed controller $K_{P\omega}$ increases from 1 to 50 ($V_w = 12$ m/s) for (a) $\lambda_{1,2}$, (b) $\lambda_{3,4}$, (c) $\lambda_{5,6}$, and (d) $\lambda_{7,8}$.

the figures indicate the directions of the eigenvalue movement as V_w increases from 8 to 15 m/s. When V_w is higher than the rated value, the power and generator speed limitation are activated, resulting in slower movement of all the eigenvalues. As shown in this figure, $\lambda_{1,2}$ move to the imaginary axis and the oscillation frequency is increased as V_w increases. For $\lambda_{3,4}$, they move away from the imaginary axis. The oscillation frequency increases up to a point ($V_w = 9$ m/s), then decreases again. For $\lambda_{5,6}$, they move to right and the oscillation frequency decreases up to a point ($V_w = 10.2$ m/s), then suddenly moves toward left. When V_w is higher than the rated value, they move to right from a new position, which is far away from imaginary axis. For $\lambda_{7,8}$, they move to left up to a point ($V_w = 11$ m/s), then they move toward right. The oscillation frequency is decreased as V_w increases. When V_w is higher than the rated value, they move to left from a new position close to imaginary axis.

TABLE III
EIGENVALUES FOR VARIATION VALUE OF V_w AND ω_r ($K_{P\omega} = 70$)

V_w (p.u.)	ω_r (p.u.)	Eigenvalues	Remarks
0.957	0.959	-7.11±j312.8, -57.0±j28.5, **0.0066±j16.7**, -6.79±j7.93, -34.2, -14.1, -4.00	Unstable
0.9568	0.9593	-7.11±j312.8, -57.0±j28.5, **0±j16.7**, -6.78±j7.92, -34.2, -14.1, -4.00	Hopf bifurcation
0.959	0.962	-7.09±j312.8, -57.0±j28.5, **-0.14±j16.3**, -6.62±j7.65, -34.2, -14.1, -4.00	Stable
1.018	1.02	-6.65±j312.9, -57.3±j27.6, **-1.61±j14.5**, -5.29±j4.80, -34.2, -14.1, -4.00	Stable
1.046	1.048	-6.45±j313.0, -56.9±j27.1, **-0.12±j17.9**, -7.36±j8.73, -34.1, -14.1, -4.00	Stable
1.0536	1.0564	-6.40±j313.0, -56.7±j27.0, **0±j19.4**, -7.71±j9.45, -34.1, -14.1, -4.000	Hopf bifurcation
1.056	1.06	-6.39±j313.0, -56.7±j27.0, **0.0038±j19.6**, -7.75±j9.53, -34.1, -14.1, -4.00	Unstable

Fig. 6(a)–(d) shows the eigenvalue loci of $\lambda_{1,2}$, $\lambda_{3,4}$, $\lambda_{5,6}$ and $\lambda_{7,8}$ as the proportional gain of rotor speed controller $K_{P\omega}$ increases from 1 to 50, respectively. $\lambda_{1,2}$ and $\lambda_{5,6}$ move toward the imaginary axis, while $\lambda_{3,4}$ and $\lambda_{7,8}$ move away from the imaginary axis as $K_{P\omega}$ increases. The oscillation frequencies of $\lambda_{1,2}$, $\lambda_{3,4}$, and $\lambda_{5,6}$ are decreased, while the oscillation frequency of $\lambda_{7,8}$ is increased as $K_{P\omega}$ increases.

The aforementioned analyses show that the operation stability of a DFIG wind turbine system can vary very much due to reasons, such as varying wind speed and control parameters. For the studied wind turbine, it is observed that as wind speed varies, $\lambda_{1,2}$ and $\lambda_{5,6}$ tend to move to the right half of the *s*-plane, if $K_{P\omega}$ is inappropriately selected above a critical value. This indicates that they are the key modes for inducing the oscillatory instability, especially when wind speed is lower than rated value. Moreover, it is obvious from the results in Fig. 5 that the system is more stable and oscillation can hardly happen when the wind speed is higher than the rated value due to activeness of the power limitation. Therefore, the oscillatory instability and eigenvalue sensitivity at higher wind speed will not been analyzed in the following section.

B. Hopf Bifurcation

Table III shows the effect of V_w and ω_r variations on the eigenvalues of the studied system when $K_{P\omega}$ is set improperly ($K_{P\omega} = 70$). It shows that there totally exist four pairs of complex conjugate eigenvalues and two real eigenvalues, as V_w and ω_r vary. When ω_r is around the synchronous speed, all these eigenvalues have negative real parts. As ω_r increases at a critical value ($\omega_r = 1.0564$ p.u.), a simple pair of pure imaginary eigenvalues $\lambda_{5,6} = 0 \pm j19.4$ of around 3 Hz appears, while other eigenvalues remain in the left half plane, and $((d(\text{Re}[\lambda(\mu)]))/d\mu)|_{\mu*} < 0$.

A supercritical HFB, therefore, occurs and a stable limit cycle emerges, leading to a smooth transition to time-periodic oscillations in the studied DFIG [19]. As ω_r increases further, the real part of the complex eigenvalues changes to positive, so the system loses stability and oscillates periodically. When ω_r decreases at a critical value ($\omega_r = 0.9593$ p.u.), a simple pair of pure imaginary eigenvalues $\lambda_{5,6} = 0 \pm j16.7$ of around 3 Hz appears, while other eigenvalues remain in the left-half

	Eigenvalue	Participation factors (%)
$\lambda_{1,2}$	$-6.84 \pm j314.0$	Pi_{ds}=26%, Pi_{qs}=26%, Pi_{dr}=24%, Pi_{qr}=24%
$\lambda_{3,4}$	$-2.76 \pm j58.8$	Pi_{ds}=10%, Pi_{dr}=11%, $P\omega_{\mathrm{r}}$=36%, $P\theta_{\mathrm{t}}$=39%
$\lambda_{5,6}$	$-5.47 \pm j29.4i$	Pi_{ds}=24%, Pi_{qs}=24%, Pi_{dr}=26%, Pi_{qr}=26%
$\lambda_{7,8}$	$-0.164 \pm j1.43$	Px_{ω}=46%, $P\omega_{\mathrm{t}}$=42%
λ_9	-34.1	PU_{dc}=71%, Px_{u}=29%
λ_{10}	-14.1	PU_{dc}=29%, Px_{u}=71%
λ_{11}	-4.00	$P\beta$=100%

plane, and $((d(\mathrm{Re}[\lambda(\mu)])/d\mu))|_{\mu*} < 0$. Therefore, a supercritical HFB occurs. As ω_r decreases further, the real part of the complex eigenvalues changes to positive and the system loses stability with periodical oscillation.

The analysis reveals that the Hopf bifurcation can happen in a DFIG wind turbine with inappropriate tuning of control parameters. For this studied system, this is essentially caused by the shift of the real part of $\lambda_{5,6}$ from negative to zero.

C. Eigenvalue Sensitivity

The eigenvalues and participation factors of the studied system when $\omega_r = 1.1$ p.u. ($V_w = 12$ m/s, $K_{P\omega} = 1$) are shown in Table IV. We can see that $\lambda_{1,2}$ are associated with the stator flux; $\lambda_{3,4}$ are associated with the rotor and turbine mechanical; $\lambda_{5,6}$ are associated with the rotor flux; $\lambda_{7,8}$ are associated with rotor and turbine mechanical; λ_9 and λ_{10} are associated with dc-link voltage; λ_{11} is associated with dynamics of pitch angle. The first-order eigenvalue sensitivities with respect to some machine and control parameters at different rotor speeds are listed in Table V. As the required perturbed parameters appear explicitly in state matrix $\mathbf{A}$, the analytical approach can be applied to compute the eigenvalue sensitivities [21].

It is obvious from Table V that a DFIG parameter differs much in their sensitivities to different eigenvalues. Furthermore, the sensitivities also vary at different rotor speeds. This observation implies that simply adjusting only one DFIG parameter cannot ensure damping enhancements of several critical eigenvalue pairs at different rotor speeds. Correspondingly, the coordinated tuning of system parameters using advanced optimization technique should be considered to improve system stability in future work.

For $\lambda_{1,2}$, the most sensitive parameters are R_s, L_{ls}, and L_{lr} as the real part of the sensitivities of $\lambda_{1,2}$ with respect to R_s, L_{ls}, and L_{lr} are larger than the others. The increase in R_s and decrease in L_{ls} and L_{lr} make $\lambda_{1,2}$ move toward left in the s-plane. For $\lambda_{3,4}$, the most sensitive parameter is H_g. A small positive perturbation in H_g makes $\lambda_{3,4}$ shift toward the imaginary axis. However, as $\lambda_{3,4}$ are not the key modes for the oscillatory stability of the studied system, the increase in H_g will not deteriorate the system stability. For $\lambda_{5,6}$, the most critical parameters are R_s, R_r, L_{ls}, and L_{lr}. The increase in R_r and decrease in L_{ls} and L_{lr} will lead to $\lambda_{5,6}$ moving toward left in the s-plane. The decrease in R_s at subsynchronous speed, while increase at synchronous and supersynchronous speed makes $\lambda_{5,6}$ shift toward left in the s-plane. For $\lambda_{7,8}$, only at synchronous

speed, $\lambda_{7,8}$ is sensitive to the variation of R_r and L_{ls}. For λ_9 and λ_{10}, the most sensitive parameters are R_r. The increase in R_r leads to λ_9 shifting toward right and λ_{10} moving toward left in the s-plane. λ_{11} is insensitive to all these parameters listed in Table V.

V. COMPUTER SIMULATION STUDY

The preceding section presents theoretical analysis based on the mathematical model. In this section, we will present a series of computer simulations to verify the theoretical analysis. In particular, we will focus on the qualitative change of dynamics as V_w is varied, as analyzed in Section IV. MATLAB/Simulink is used to establish the simulation model of DFIG system described in the foregoing section. All the components of the simulation model are built with standard electrical component blocks from the SimPowerSystems block set in MATLAB/Simulink library.

A. Stable Operation

Fig. 7(a)–(f) shows the time-domain waveforms of rotor speed ω_r, dc-link voltage U_{dc}, active power P, reactive power Q, stator current of phase A i_{sa} and rotor current of phase A i_{ra} when wind speed $V_w = 11.1$ m/s, rotor speed set point $\omega_{\mathrm{ref}} = 1.015$. It is shown that ω_r, U_{dc}, P, and Q are nearly constant, i_{sa} and i_{ra} are sinusoidal. The system is stable and there is no oscillatory behavior.

B. Oscillatory Instability

When V_w varies above a critical value, oscillatory behavior can occure in the studied system. Fig. 8 shows the corresponding steady-state time-domain waveforms, after a step increase of 0.9 m/s (8.1%) is applied to V_w ($V_w = 12$ m/s, $\omega_{\mathrm{ref}} \approx 1.1$). It is shown that ω_r, U_{dc}, P, and Q are no longer constant, but oscillate around the frequency of 3 Hz. i_{sa} and i_{ra} are no more sineusoidal. In Section III, the nature of such oscillation is analyzed from a Hopf bifurcation perspective. It can be observed that Hopf bifurcation takes place at approximately the same wind speed condition as it does in our theoretical analysis, and the simulated periodic oscillations also match the earlier Hopf bifurcation analysis.

C. Hopf Bifurcation Boundary

The analysis in Section IV already shows that the oscillatory instability is essentially Hopf bifurcation induced one, through the eigenvalues $\lambda_{5,6}$. Sensitivity analysis also indicates the parameters, which have significant effects on the movement of $\lambda_{5,6}$, are R_s, R_r, L_{ls}, and L_{lr}. In this section, the stability boundary curves with respect to those critical parameters within the space of $K_{P\omega}$ versus ω_r, where the conjugate eigenvalues $\lambda_{5,6}$ intersecting with the imaginary axis are mapped, which corrospond to the occurence of Hopf bifurcation. The Hopf bifurcation boundaries can be readily obtained by using the analytical means described in the earlier section. On the other hand, the boundaries obtained from simulations performed in MATLAB/Simulink are also given to verify the results from theoretical analysis.

TABLE V
FIRST-ORDER EIGENVALUES SENSITIVITIES GIVEN DIFFERENT ROTOR SPEED: (A) $\omega_r = 0.9$ SUBSYNCHRONOUS SPEED;
(B) $\omega_r = 1$ SYNCHRONOUS SPEED; (C) $\omega_r = 1.1$ SUBSYNCHRONOUS SPEED

(A)

	$\lambda_{1,2}$	$\lambda_{3,4}$	$\lambda_{5,6}$	$\lambda_{7,8}$	λ_9	λ_{10}	λ_{11}
R_s	-107±j14.7	-0.203±j1.67	91.8±j12.0	-0.103±j0.0256	0	0	0
R_r	0.0843±j26.9	-0.209±j1.66	-984.6±j28.2	-9.05e^{-3}±j0.0837	10.5	-4.131	0
L_{ls}	25.5±j0.749	0.0625±j0.887	11.7±j0.425	0.0256±j0.00871	0.115	-0.0451	0
L_{lr}	23.4±j0.757	5.11e^{-4}±j0.0123	13.3±j0.716	2.53e^{-3}±j0.000736	0	0	0
L_m	0.0444±j0.00382	0.227±j0.363	-0.102±j0.167	-0.0931±j0.0106	0.363	-0.142	0
H_g	-4.84e^{-3}±j0.0432	6.43±j66.8	0.0253±j0.0144	0.0348±j0.160	0	0	0
H_t	0	0.0412±j0.660	-0.0137±j0.00152	0.0354±j0.161	0	0	0
$K_{P\omega}$	1.69e^{-3}±j0.0168	-0.585±j0.0664	0.0623±j0.00124	-0.104±j0.712	0	0	0
$T_{i\omega}$	5.32e^{-3}±j5.61e^{-4}	-0.0134±j0.892	4.58e^{-3}±j0.00483	3.47e^{-3}±j7.23	0	0	0

(B)

	$\lambda_{1,2}$	$\lambda_{3,4}$	$\lambda_{5,6}$	$\lambda_{7,8}$	λ_9	λ_{10}	λ_{11}
R_s	-978.4±j16.8	-0.255±j0.335	-2.05±j14.2	-0.0169±j0.0188	0	0	0
R_r	0.221±j22.2	0.0795±j0.822	-984.1±j22.5	-0.936±j2.35	14.2	-5.58	0
L_{ls}	23.2±j0.731	0.0795±j0.984	12.9±j0.547	1.14±j0.169	0.0100	-0.00394	0
L_{lr}	21.3±j 0.728	-3.04e^{-3}±j5.80e^{-3}	15.5±j0.677	0.0123±j 0.0374	0	0	0
L_m	0.0396±j0.00371	-0.0279±j0.273	0.303±j0.642	-0.239±j0.0188	-0.0391	0.0154	0
H_g	-6.88e^{-3}±j0.0396	6.47±j66.8	-0.0110±j1.00e^{-4}i	0.0353±j0.164	0	0	0
H_t	0	0.0387±j0.661	-0.0103±j1.00e^{-4}i	0.0359±j0.166	0	0	0
$K_{P\omega}$	2.49e^{-3}±j0.0153	-0.571±j0.0588	0.0443±j3.30e^{-4}	-0.101±j0.732	0	0	0
$T_{i\omega}$	4.87e^{-3}±j8.25e^{-4}	1.09e^{-3}±j0.891	0.0349±j0.0344	-0.0409±j7.29	0	0	0

(C)

	$\lambda_{1,2}$	$\lambda_{3,4}$	$\lambda_{5,6}$	$\lambda_{7,8}$	λ_9	λ_{10}	λ_{11}
R_s	-900.2±j17.4	-0.358±j0.800	-80.3±j15.1	0.0908±j0.0211	0	0	0
R_r	0.273±j18.7	0.753±j1.76	-985.7±j17.3	-0.0254±j0.0663	18.9	-7.47	0
L_{ls}	21.3±j0.695	0.234±j1.81	15.7±j1.26	0.0403±j0.0159	-0.307	0.121	0
L_{lr}	19.5±j0.684	-0.0168±j0.0470	17.3±j0.611	-1.86e^{-3}±j0.00160	0	0	0
L_m	0.0353±j0.00351	-0.437±j0.321	0.373±j0.0127	0.105±j0.00833	-0.606	0.239	0
H_g	-9.29e^{-3}±j0.0365	6.43±j66.8	0.0266±j0.0252	0.0368±j0.159	0	0	0
H_t	0	0.0418±j0.660	-0.0135±j 0.00107	0.0373±j0.161	0	0	0
$K_{P\omega}$	3.43e^{-3}±j0.0142	-0.588±j 0.0473	0.0623±j0.00943	-0.103±j0.712	0	0	0
$T_{i\omega}$	4.50e^{-3}±j0.00113	0.0121±j0.892	-4.83e^{-3}±j0.00201	-0.0118±j 7.24	0	0	0

Fig. 9(a)–(d) shows the Hopf bifurcation boundaries in the parameter space of $K_{P\omega}$ versus ω_r under different values of R_s, R_r, L_{ls}, and L_{lr}, respectively, which clearly illustrates the effect of those sensitive parameters on the Hopf bifurcation boundaries. Area below the curves corresponds to stable operation and above that to unstable operation. On top of these curves, the system loses stability via Hopf bifurcation.

As shown in Fig. 9, the simulation results agree well with the analytical results. Also, we can generally observe that around synchronous speed, the critical value of $K_{P\omega}$ is the largest, and does not change so significantly in different system parameter conditions. When ω_r is away from synchronous speed (e.g., in 0.7–0.9 or around 1.1), the critical value of $K_{P\omega}$ decreases as the value of ω_r increases, and Hopf bifurcation boundaries have considerable changes in different system parameter conditions. The point marked with "∗" is the stable operating point before the bifurcation occurs. At subsynchronous speed, the Hopf bifurcation margin becomes smaller as R_s increases. While at supersynchronous speed, the Hopf bifurcation margin becomes larger as R_s increases. For all studied region of rotor speed, the Hopf bifurcation margin becomes larger, as R_r increases, while L_{ls} and L_{lr} decrease.

D. Discussion

The simulation results have confirmed the theoretical analysis based on derived model and Jacobian matrix. The simulation results show that the oscillatory behavior with the nature of Hopf bifurcation can happen due to reason like varying wind speed. The observed oscillation is primarily due to the varying electromagnetic torque, since the mechanical one is fixed. Such oscillation of the electromagnetic torque is related to the variations of the magnitude and direction of the stator and rotor flux-linkage vectors [22], [23], which is not focused herein, but will be investigated in our future scope.

Besides the wind speed and control parameters, Hopf bifurcation is also sensitive to other system parameters, and the impact of different parameters on the Hopf bifurcation margin at different rotor speeds is different. For the studied system, Hopf bifurcation boundaries for the eigenvalues $\lambda_{5,6}$ show that such bifurcation can happen particularly when R_s, L_{ls}, and L_{lr} increase, while R_r decreases at subsynchronous speed. At supersynchronous speed, the increase of L_{ls} and L_{lr}, while decrease of R_s and R_r may lead to such Hopf bifurcation. Hence, simply increasing R_s cannot enhance the Hopf bifurcation margin at different rotor speeds, and it is recommended to choose large value of R_r, while small value of L_{ls} and L_{lr} to enlarge such Hopf bifurcation margin. These are the important characteristics for a DFIG wind turbine system, and very useful for the operators of such system to be careful in situations, where critical parameters may be changed. Hopf bifurcation boundaries for other eigenvalues have also been studied. Though different bifurcation boundaries will be exhibited for different eigenvalues,
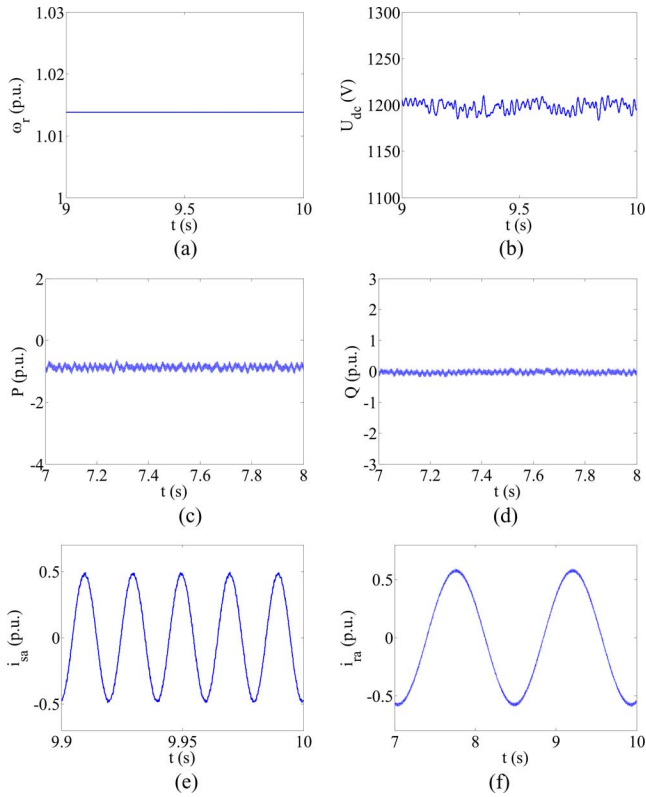
Fig. 7. Simulation results when DFIG works in stable operation. (a) Rotor speed ω_r. (b) DC-link voltage U_{dc}. (c) Active power P. (d) Reactive power Q. (e) Phase A of stator current i_{sa}. (f) Phase A of rotor current i_{ra}.

Fig. 8. Simulation results when oscillatory instability occurs. (a) Rotor speed ω_r. (b) DC-link voltage U_{dc}. (c) Active power P. (d) Reactive power Q. (e) Phase A of stator current i_{sa}. (f) Phase A of rotor current i_{ra}.
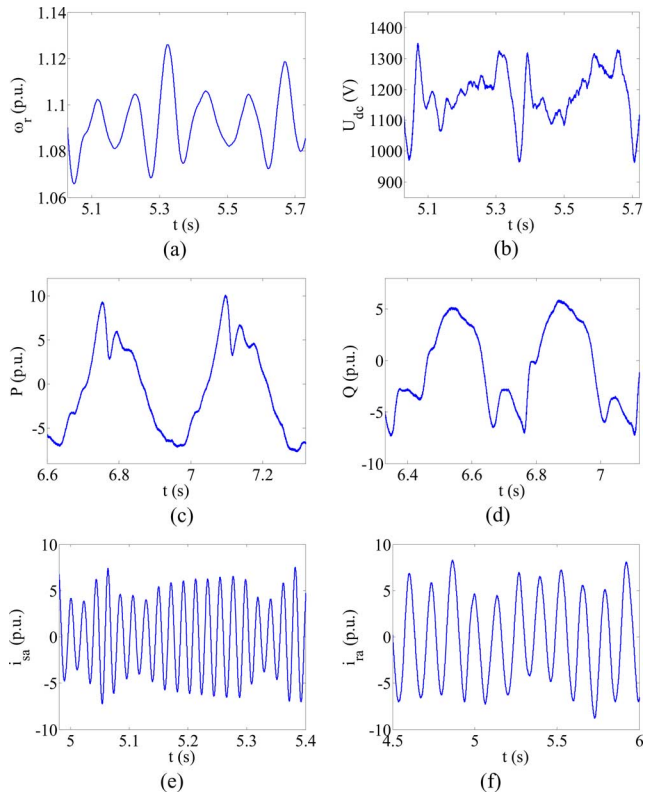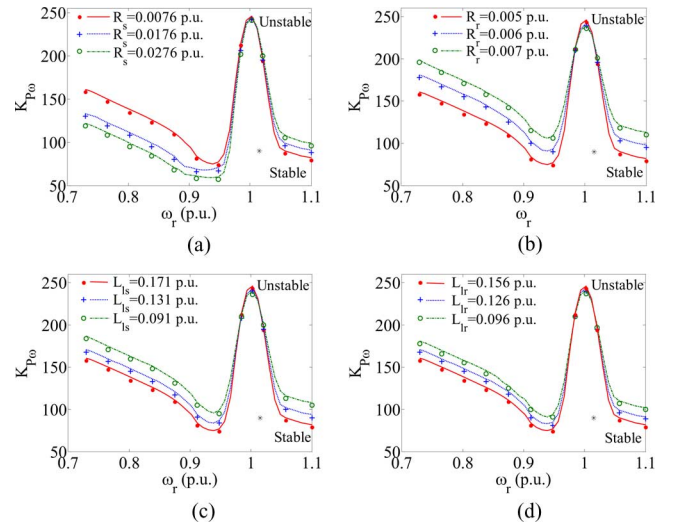

Fig. 9. Hopf bifurcation boundaries in the parameter space of $K_{P\omega}$ versus ω_r for (a) different values of stator resistance R_s, (b) mutual inductance R_r, (c) stator leakage inductance L_{ls}, and (d) rotor leakage inductance L_{lr}. Results from analysis are denoted by the solid line. Results from simulations are represented by "●", "+," and "○". The dot "∗" is the stable operating point.

in general, a varying style along with rotor speed can be clearly observed.

When the wind speed is higher than the rated value, the power limitation is activated. It is obvious from the results in Fig. 5 that the system is more stable and Hopf bifurcation can hardly happen. Therefore, the bifurcation boundary at higher wind speed has not been analyzed in this paper.

VI. CONCLUSION

DFIG has been one of the popular types for high-power applications of wind power generation. However, the detailed nonlinear dynamics of this system, so far, has not been thoroughly investigated. In this paper, a detailed DFIG wind turbine model including two-mass drive train, pitch control, induction generator, back-to-back PWM converters, and vector-control loops was developed. The Jacobian matrix was also derived for small-signal-stability analysis purpose. Bifurcation and eigenvalue sensitivity analysis based on both theoretical analysis and computer simulations showed that DFIG wind turbine can loose stability via a Hopf bifurcation. Further analysis showed that the impact of different DFIG parameters on different critical eigenvalue pairs at different rotor speeds was different. The most sensitive parameters to the Hopf bifurcation of a DFIG wind turbine system can be identified through eigenvalue sensitivity analysis. Moreover, the Hopf bifurcation boundaries with respect to those critical parameters have also been analyzed that can facilitate parameterizing the DFIG wind turbine system to ensure stable operation. The analyses in this paper provide insights into DFIG oscillatory stability that can be important for both manufacturer and system operators in designing or practically operating such wind turbines concerning their impact on power system small-signal stability.

<div align="center">

APPENDIX

JACOBIAN MATRIX

</div>

$$J_{11} = D\left(R_s L_r + L_m \frac{\partial u_{dr}}{\partial i_{ds}}\right) \quad J_{112} = D L_m \frac{\partial u_{dr}}{\partial x_{us}}$$

$$J_{12} = D\left[(\omega_s - \omega_{r0})L_m^2 - \omega_s L_s L_r + L_m \frac{\partial u_{dr}}{\partial i_{qs}})\right]$$

$$J_{13} = D\left(-R_r L_m + L_m \frac{\partial u_{dr}}{\partial i_{dr}}\right)$$

$$J_{14} = D\left[-\omega_{r0} L_r L_m + L_m \frac{\partial u_{dr}}{\partial i_{qr}})\right]$$

$$J_{15} = D\left[-L_m^2 I_{qs0} - L_r L_m I_{qr0} + L_m \frac{\partial u_{dr}}{\partial \omega_r})\right]$$

$$J_{17} = D L_m \frac{\partial u_{dr}}{\partial x_\omega} \quad J_{19} = D L_m \frac{\partial u_{dr}}{\partial \theta_\omega}$$

$$J_{110} = D L_m \frac{\partial u_{dr}}{\partial \omega_t} \quad J_{111} = D L_m \frac{\partial u_{dr}}{\partial \beta}$$

$$J_{21} = D\left[-(\omega_s - \omega_{r0})L_m^2 + \omega_s L_s L_r + L_m \frac{\partial u_{qr}}{\partial i_{ds}})\right]$$

$$J_{22} = D\left(R_s L_r + L_m \frac{\partial u_{qr}}{\partial i_{qs}}\right)$$

$$J_{23} = D\left[\omega_{r0} L_r L_m + L_m \frac{\partial u_{qr}}{\partial i_{dr}})\right]$$

$$J_{24} = D\left(-R_r L_m + L_m \frac{\partial u_{qr}}{\partial i_{qr}}\right) \quad J_{27} = D L_m \frac{\partial u_{qr}}{\partial x_\omega}$$

$$J_{29} = D L_m \frac{\partial u_{qr}}{\partial \theta_\omega}$$

$$J_{25} = D\left[L_m^2 I_{ds0} + L_r L_m I_{dr0} + L_m \frac{\partial u_{qr}}{\partial \omega_r})\right]$$

$$J_{210} = D L_m \frac{\partial u_{qr}}{\partial \omega_t} \quad J_{211} = D L_m \frac{\partial u_{qr}}{\partial \beta}$$

$$J_{212} = D L_m \frac{\partial u_{qr}}{\partial x_{us}} \quad J_{31} = D(-R_s L_m - L_s \frac{\partial u_{dr}}{\partial i_{ds}})$$

$$J_{32} = D\left[\omega_{r0} L_s L_m - L_s \frac{\partial u_{dr}}{\partial i_{qs}})\right]$$

$$J_{33} = D\left(R_r L_s - L_s \frac{\partial u_{dr}}{\partial i_{dr}}\right)$$

$$J_{34} = D\left[\omega_s L_m^2 - (\omega_s - \omega_{r0})L_s L_r - L_s \frac{\partial u_{dr}}{\partial i_{qr}})\right]$$

$$J_{35} = D\left[L_s L_m I_{qs0} + L_s L_r I_{qr0} - L_s \frac{\partial u_{dr}}{\partial \omega_r})\right]$$

$$J_{37} = -D L_s \frac{\partial u_{dr}}{\partial x_\omega} \quad J_{39} = D L_m \frac{\partial u_{dr}}{\partial \theta_\omega}$$

$$J_{310} = -D L_s \frac{\partial u_{dr}}{\partial \omega_t} \quad J_{311} = -D L_s \frac{\partial u_{dr}}{\partial \beta}$$

$$J_{312} = -D L_s \frac{\partial u_{dr}}{\partial x_{us}} \quad J_{41} = D\left(-\omega_{r0} L_s L_m - L_s \frac{\partial u_{qr}}{\partial i_{ds}}\right)$$

$$J_{42} = D\left(-R_s L_m - L_s \frac{\partial u_{qr}}{\partial i_{qs}}\right) \quad J_{44} = D\left(R_r L_s - L_s \frac{\partial u_{qr}}{\partial i_{qr}}\right)$$

$$J_{43} = D\left[-\omega_s L_m^2 + (\omega_s - \omega_{r0})L_s L_r - L_s \frac{\partial u_{qr}}{\partial i_{dr}})\right]$$

$$J_{45} = D\left[-L_s L_m I_{ds0} - L_s L_r I_{dr0} - L_s \frac{\partial u_{qr}}{\partial \omega_r})\right]$$

$$J_{47} = -D L_s \frac{\partial u_{qr}}{\partial x_\omega} \quad J_{49} = -D L_s \frac{\partial u_{qr}}{\partial \theta_\omega}$$

$$J_{410} = -D L_s \frac{\partial u_{qr}}{\partial \omega_t} \quad J_{411} = -D L_s \frac{\partial u_{qr}}{\partial \beta}$$

$$J_{412} = -D L_s \frac{\partial u_{qr}}{\partial x_{us}} \quad J_{51} = -\frac{L_m}{2H_g} I_{qr0}$$

$$J_{52} = \frac{L_m}{2H_g} I_{dr0} \quad J_{53} = \frac{L_m}{2H_g} I_{qs0} \quad J_{54} = -\frac{L_m}{2H_g} I_{ds0}$$

$$J_{55} = -\frac{D_{\text{sh}}\omega_b + B}{2H_g} \quad J_{59} = \frac{K_{\text{sh}}}{2H_g} \quad J_{510} = \frac{D_{\text{sh}}\omega_b}{2H_g}$$

$$J_{61} = -\frac{1}{G_0}\left(I_{dr0} \frac{\partial u_{dr}}{\partial i_{ds}} + I_{qr0} \frac{\partial u_{qr}}{\partial i_{ds}}\right)$$

$$J_{62} = -\frac{1}{G_0}\left(I_{dr0} \frac{\partial u_{dr}}{\partial i_{qs}} + I_{qr0} \frac{\partial u_{qr}}{\partial i_{qs}}\right)$$

$$J_{63} = -\frac{1}{G_0}\left(U_{dr0} + I_{dr0} \frac{\partial u_{dr}}{\partial i_{dr}} + I_{qr0} \frac{\partial u_{qr}}{\partial i_{dr}}\right)$$

$$J_{64} = -\frac{1}{G_0}\left(U_{qr0} + I_{dr0} \frac{\partial u_{dr}}{\partial i_{qr}} + I_{qr0} \frac{\partial u_{qr}}{\partial i_{qr}}\right)$$

$$J_{65} = -\frac{1}{G_0}\left(I_{dr0} \frac{\partial u_{dr}}{\partial \omega_r} + I_{qr0} \frac{\partial u_{qr}}{\partial \omega_r}\right)$$

$$J_{66} = -\frac{W_0}{G_0^2} \frac{\partial G}{\partial U_{\text{dc}}} + \frac{\partial W}{G_0 \partial U_{\text{dc}}}$$

$$J_{67} = -\frac{1}{G_0}\left(I_{dr0} \frac{\partial u_{dr}}{\partial x_\omega} + I_{qr0} \frac{\partial u_{qr}}{\partial x_\omega}\right)$$

$$J_{68} = -\frac{W_0}{G_0^2} \frac{\partial G}{\partial x_u} + \frac{\partial W}{G_0 \partial x_u}$$

$$J_{69} = -\frac{1}{G_0}\left(I_{dr0} \frac{\partial u_{dr}}{\partial \theta_\omega} + I_{qr0} \frac{\partial u_{qr}}{\partial \theta_\omega}\right)$$

$$J_{610} = -\frac{1}{G_0}\left(I_{dr0} \frac{\partial u_{dr}}{\partial \omega_t} + I_{qr0} \frac{\partial u_{qr}}{\partial \omega_t}\right)$$

$$J_{611} = -\frac{1}{G_0}\left(I_{dr0} \frac{\partial u_{dr}}{\partial \beta} + I_{qr0} \frac{\partial u_{qr}}{\partial \beta}\right)$$

$$J_{612} = -\frac{1}{G_0}\left(I_{dr0} \frac{\partial u_{dr}}{\partial x_{us}} + I_{qr0} \frac{\partial u_{qr}}{\partial x_{us}}\right)$$

$$J_{75} = -\frac{K_{P\omega}}{T_{I\omega}} \quad J_{710} = \frac{K_{P\omega}}{2T_{I\omega}}\left(\frac{T_m}{K_{opt}}\right)^{-0.5} \frac{\partial T_m}{\partial \omega_t}$$

$$J_{86} = -\frac{K_{Pv}}{T_{Iv}} \quad J_{711} = \frac{K_{P\omega}}{2T_{I\omega}} \left(\frac{T_m}{K_{\text{opt}}}\right)^{-0.5} \frac{\partial T_m}{\partial \beta}$$

$$J_{95} = -\omega_b \quad J_{910} = \omega_b$$

$$J_{105} = \frac{D_{\text{sh}}\omega_b}{2H_t} \quad J_{109} = -\frac{K_{\text{sh}}}{2H_t}$$

$$J_{1010} = \frac{1}{2H_t}\left(\frac{\partial T_m}{\partial \omega_t} - D_{\text{sh}}\omega_b\right) \quad J_{1011} = \frac{1}{2H_t}\frac{\partial T_m}{\partial \beta}$$

$$J_{1101} = \frac{1}{T_\beta}\frac{\partial \beta_{\text{ref}}}{\partial i_{ds}} \quad J_{1102} = \frac{1}{T_\beta}\frac{\partial \beta_{\text{ref}}}{\partial i_{qs}}$$

$$J_{116} = \frac{1}{T_\beta}\frac{\partial \beta_{\text{ref}}}{\partial U_{\text{dc}}} \quad J_{118} = \frac{1}{T_\beta}\frac{\partial \beta_{\text{ref}}}{\partial x_u}$$

$$J_{1111} = -\frac{1}{T_\beta} \quad J_{1113} = \frac{1}{T_\beta}\frac{\partial \beta_{\text{ref}}}{\partial x_\beta}$$

$$J_{131} = \frac{K_{P\beta}}{T_{I\beta}}\frac{\partial P_g}{\partial i_{ds}} \quad J_{132} = \frac{K_{P\beta}}{T_{I\beta}}\frac{\partial P_g}{\partial i_{qs}}$$

$$J_{136} = \frac{K_{P\beta}}{T_{I\beta}}\frac{\partial P_g}{\partial U_{\text{dc}}} \quad J_{138} = \frac{K_{P\beta}}{T_{I\beta}}\frac{\partial P_g}{\partial x_u},$$

$$\text{where } G = \frac{2C_{\text{dc}}}{3\omega_b}U_{\text{dc}} - \frac{\sqrt{2}LK_{Pv}}{\sqrt{3}m\omega_b}i_{dL}^\varepsilon$$

$$W = i_{dL}^\varepsilon \left[U_s - R_L i_{dL}^\varepsilon - \frac{\sqrt{2}LK_{Pv}}{\sqrt{3}m\omega_b T_{Iv}}(U_{\text{dcref}} - U_{\text{dc}})\right.$$
$$\left. + \omega_s L I_{qL\text{ref}}\right] - I_{qL\text{ref}}(R_L I_{qL\text{ref}} + \omega_s L i_{dL}^\varepsilon)$$
$$- (u_{dr}i_{dr} + u_{qr}i_{qr}).$$

References

[1] J. Nagy, L. Matakas, and E. Masada, "Application of the theory of chaos in PWM technique of induction motors," in *Proc. Int. Conf. Power Electron.*, 1995, pp. 58–63.
[2] J. H. Chen, K. T. Chau, and C. C. Chan, "Analysis of chaos in current-mode-controlled dc drive systems," *IEEE Trans. Ind. Electron.*, vol. 47, no. 1, pp. 67–76, Feb. 2000.
[3] Z. Li, J. B. Park, Y. H. Joo, B. Zhang, and G. R. Chen, "Bifurcation and chaos in a permanent-magnet synchronous motor," *IEEE Trans. Circuits Syst. I, Fundam. Theory Appl.*, vol. 49, no. 3, pp. 383–387, Mar. 2002.
[4] Y. Gao and K. T. Chau, "Hopf bifurcation and chaos in synchronous reluctance motor drives," *IEEE Trans. Energy Convers.*, vol. 19, no. 2, pp. 296–302, Jun. 2004.
[5] F. Mei and B. C. Pal, "Modal analysis of grid-connected doubly fed induction generators," *IEEE Trans. Energy Convers*, vol. 22, no. 3, pp. 728–736, Sep. 2007.
[6] F. Wu, X. P. Zhang, K. Godfrey, and P. Ju, "Small signal stability analysis and optimal control of a wind turbine with doubly fed induction generator," *IET Gen. Trans. Distr.*, vol. 1, no. 5, pp. 751–760, 2007.
[7] C. Wang and L. Shi, "Small signal stability analysis considering grid-connected wind farms of DFIG type," in *Proc. IEEE Power and Energy Soc. Gen. Meeting*, Jul. 2008, pp. 20–24.
[8] G. Tsourakis, B. M. Nomikos, and C. D. Vournas, "Effect of wind parks with doubly fed asynchronous generators on small-signal stability," *Electr. Power Syst. Res.*, vol. 79, pp. 190–200, 2009.
[9] L. Yang, X. Ma, and D. Dai, "Hopf bifurcation in doubly fed induction generator under vector control," *Chaos, Sol. Fract.*, vol. 41, no. 5, pp. 2741–2749, 2009.
[10] A. D. Hansen, P. Sørensen, F. Iov, and F. Blaabjerg, "Control of variable speed wind turbines with doubly-fed induction generators," *Wind Eng.*, vol. 28, no. 4, pp. 411–434, 2004.
[11] C. W. Liu, H. Q. Weng, X. D. Sun, and F. H. Li, "Research of stability of double fed induction motor vector control system," in *Proc. 5th Int. Conf. on Electr. Machines Syst.*, Aug. 2001, vol. 2, pp. 1203–1206.
[12] P. Pourbeik (convener), WG C4.601, "Modeling and dynamic behavior of wind generation as it relates to power system control and dynamic performance," CIGRE, Paris, France, Tech. Brochure 328, Aug. 2007.
[13] L. Rouco and J. L. Zamora, "Dynamic patterns and model order reduction in small-signal models of doubly fed induction generators for wind power applications," in *Proc. IEEE PES Gen. Meeting*, 2006, pp. 1–8.
[14] P. C. Krause, O. Wasynczuk, and S. D. Sudhoff,, *Analysis of Electric Machinery and Drive Systems*. Piscataway, NJ: IEEE Press, 2002.
[15] V. Akhmatov, *Induction Generators for Wind Power*. Brentwood, Essex, U.K: Multi-science Publ. Co. Ltd, 2005.
[16] R. Cardenas, "Control of wind turbines using switched reluctance generators," Ph.D. thesis, Univ. Nottingham, U.K., 1996.
[17] R. Pena, J. C. Clare, and G. M. Asher, "Doubly fed induction generator using back-to-back PWM converters and its application to variable speed wind-energy generation," in *Proc. Inst. Elect. Eng. Electr. Power Appl.*, May 1996, vol. 143, no. 3, pp. 231–241.
[18] P. Ledesma and J. Usaola, "Doubly fed induction generator model for transient stability analysis," *IEEE Trans. Energy Convers.*, vol. 20, no. 2, pp. 388–397, Jun. 2005.
[19] Z. Y. Dong, "Advanced methods for power system small signal stability and control," Ph.D. thesis, Sydney Univ., Sydney, Australia, 1999, pp. S4–S57.
[20] J. Ma and Z. Y. Dong, "Eigenvalue Sensitivity Analysis for Probabilistic Small Signal Stability Assessment," presented at the IET APSCOM'06, Hong Kong, China.
[21] Z. Y. Dong, C. K. Pang, and P. Zhang, "Power System Sensitivity Analysis for Probabilistic Small Signal Stability Assessment in a Deregulated Environment," *Int. J. Control, Automat. Syst.*, vol. 3, no. 2, pp. 355–362, Jun. 2005.
[22] M. Alakula, B. Peterson, and J. Valis, "Damping of oscillations in induction machines," in *Proc. 23rd Annu. IEEE Power Electron. Spec. Conf.*, Jun. 1992, vol. 1, pp. 133–138.
[23] J. Zhang, M. F. Rahman, and L. Tang, "Modified direct torque controlled induction generator with space vector modulation for integrated starter alternator," in *Proc. 4th Int. Power Electron. Motion Control Conf.*, Aug. 2004, vol. 1, pp. 405–408.

Lihui Yang received the Ph.D. degree in electrical engineering from Xi'an Jiaotong University, Xi'an, Shaanxi, China, in 2010.

During 2008–2009, she was a Visiting Ph.D. Student at the Center for Electric Technology, Technical University of Denmark. She is currently an Assistant Professor at Xi'an Jiaotong University. Her research interests include stability and control of wind power generation.

Zhao Xu (S'00–M'06) received the Ph.D. degree in electrical engineering from The University of Queensland, Australia, in 2006.

From 2006–2009, he was an Assistant at the Center for Electric Technology, Technical University of Denmark, where he became an Associate Professor. Since 2010, he has been with Hong Kong Polytechnic University, Kowloon, Hong Kong. His research interests include demand side, grid integration of wind power, electricity market planning and management, and AI applications.

Jacob Østergaard (M'95–SM'09) received the M.Sc. degree in electrical engineering from the Technical University of Denmark, Lyngby, Denmark, in 1995.

He is currently a Professor and the Head of the Center for Electric Technology, Department of Electrical Engineering, Technical University of Denmark. His research interests include integration of renewable energy, control architecture for future power system, and demand side.

Prof. Østergaard is engaged with several professional organizations, including the EU SmartGrids Advisory Council.

Kit Po Wong (M'87–SM'90–F'02) received the M.Sc., Ph.D., and D.Eng. degrees from the Institute of Science and Technology, University of Manchester, Manchester, U.K., in 1972, 1974, and 2001, respectively.

From 1974 to 2004, he was at The University of Western Australia, Perth, Australia, where he is currently an Adjunct Professor. He was the Head of the Department of Electrical Engineering, The Hong Kong Polytechnic University, Kowloon, Hong Kong, where he has been the Chair Professor, since 2002. His research interests include computation intelligence applications to power system analysis, planning and operations, as well as power market analysis.

Prof. Wong received three Sir John Madsen Medals (1981, 1982, and 1988) from the Institution of Engineers, Australia (IEAust), the 1999 Outstanding Engineer Award from IEEE Power Chapter Western Australia, and the 2000 IEEE Third Millennium Award. He was a Co-Technical Chairman of the IEEE International Conference on Machine Learning and Cybernetics (ICMLC) 2004 and the General Chairman of IEEE/CSEE PowerCon2000. He was an Editor-in-Chief of *IEE Proceedings in Generation*, *Transmission and Distribution* and the Editor (Electrical) of the *Transactions of Hong Kong Institution of Engineers*. He is a Fellow of the Institution of Engineering and Technology (IET), the Hong Kong Institution of Engineers (HKIE), and the IEAust.

Zhao Yang Dong (M'99–SM'06) received the Ph.D. degree from The University of Sydney, Sydney, Australia, in 1999.

He was engaged in various academic positions at The University of Queensland, Australia and National University of Singapore. He is currently engaged at Hong Kong Polytechnic University, Kowloon, Hong Kong. He is also engaged in various industrial positions with Powerlink Queensland, Virginia, and Transend Networks, Tasmania, Australia (both are transmission network service providers in corresponding states). His research interests include power system planning, power system security assessment, power system stability and control, power system load modeling, electricity market, and computational intelligence and its application in power engineering.

Xikui Ma received the B.E. and M.Sc. degrees in electrical engineering from Xi'an Jiaotong University, Xi'an, China, in 1982 and 1985, respectively.

In 1985, he joined the Xi'an Jiaotong University as a Lecturer, where he has been a Professor, since 1992. His current research interests include electromagnetic field theory and its application, numerical methods, modeling of magnetic components, chaotic dynamics and its applications in power electronics, and applications of digital control in power electronics.